Supporting Information for "Contrasting responses to orbital precession on Titan and Earth"

Junjun Liu[1] and Tapio Schneider[1,2]

Contents of this file

1. Text S1 to S3
2. Figure S1 to S4

Introduction

This supporting information provides more detailed descriptions of the model setup (Figs. S1 and S2), of components of the meridional methane transport (Fig. S3), and of the response of the atmospheric meridional methane transport to orbital precession (Fig. S4).

Corresponding author: Tapio Schneider, California Institute of Technology, Pasadena, California, USA (tapio@caltech.edu)

[1]California Institute of Technology,

Pasadena, California, USA.

[2]ETH Zurich, Zurich, Switzerland

Text S1: : Model setup

The Titan GCM used in this study is based on the Flexible Modeling System of the Geophysical Fluid Dynamics Laboratory (http://fms.gfdl.noaa.gov), with Titan's physical parameters and with a methane cycle instead of a water cycle. The model is described in *Schneider et al.* [2012] and is available from climate-dynamics.org. Here we only state differences to that earlier study.

1. Resolution

The Titan GCM uses the spectral transform method in the horizontal and finite difference in the vertical. The horizontal spectral resolution is T42 (corresponding to about $2.5^\circ \times 2.5^\circ$ resolution in the Gaussian transformed grid), which is higher than the horizontal resolution of T21 used in *Schneider et al.* [2012]. The vertical coordinate is $\sigma = p/p_s$ (pressure p normalized by the surface pressure p_s) with 18 levels. As a slight difference from the GCM in *Schneider et al.* [2012], here we use the modified Robert-Asselin-Williams filter to reduce the numerical errors produced in the leap-frog time stepping scheme [*Williams*, 2011].

2. Radiative transfer

Similar to the Titan GCM in *Schneider et al.* [2012], radiative transfer is represented using the two-stream approximation. We use slightly different radiative parameters to better fit the observed bond albedo and solar heat flux [*Tomasko and Smith*, 1982; *Neff et al.*, 1985; *Tomasko et al.*, 2008], and to correct coding errors we discovered in the implementation of the radiative transfer scheme used in *Schneider et al.* [2012].

At the top of the atmosphere, Saturn's seasonally varying insolation is imposed with no diurnal cycle. Solar radiation is scattered and absorbed in the atmosphere, assuming diffuse incidence and multiple scattering, with asymmetry factor 0.6 and single scattering albedo of 0.85. The solar optical depth is specified as:

$$\tau_s = \tau_{s0} \left(\frac{p}{p_0} \right)^{\gamma}, \tag{1}$$

with optical thickness $\tau_{s0} = 3.3$ at $p_0 = 1.467 \times 10^5$ Pa and empirical exponent $\gamma = 0.28$. The surface albedo is 0.3 uniformly. The planetary bond albedo is 0.29, which is consistent with the observed value [*Tomasko and Smith*, 1982; *Neff et al.*, 1985]. The model's net solar radiative fluxes fit well the ones measured by the Huygen probe [*Tomasko et al.*, 2008] (Fig. S1).

Longwave radiation is absorbed in the atmosphere, with an optical depth

$$\tau_l = \tau_{l0} \left[\alpha \left(\frac{p}{p_0} \right) + (1 - \alpha) \left(\frac{p}{p_0} \right)^2 \right], \tag{2}$$

which roughly represents a mixture of absorption by a well-mixed absorber (linear dependence on pressure) and collision induced absorption (quadratic dependence on pressure). Here $\alpha = 0.05$, and the longwave optical thickness of the atmosphere is taken to be $\tau_{l0} = 14$.

In the statistically steady state of the simulations, this formulation of radiative transfer results in a realistic temperature profile with a tropopause. Compared with temperatures measured by the Huygens probe, the temperatures in the simulations are within 1 K in the lower troposphere and within 6 K near the tropopause (Fig. S2).

3. Methane reservoir

The simulation is initialized with a dry surface and with an isothermal (86 K) atmosphere containing the equivalent of 12 m of liquid methane distributed uniformly. The total methane concentration is conserved in the simulations up to small numerical inaccuracies. In the statistically steady state, the seasonally and globally averaged methane concentration in the atmosphere corresponds to ~ 8 m liquid methane in the simulations with Titan's rotation rate and ~ 7.5 m liquid methane in the simulations with Earth's rotation rate. These values are slightly higher than the atmospheric methane concentration (~ 7 m) in T21 simulations with similar parameters. The remaining methane is on the surface.

4. Subgrid scale dissipation

Horizontal ∇^8 hyperdiffusion in the vorticity, divergence, temperature, and specific humidity equations represents unresolved turbulent dissipation. The hyperdiffusion coefficient is chosen to give a damping time scale of 2.4 hrs at the smallest resolved scale.

Text S2: Decomposition of meridional methane transport

Following Section 3 in the main text, in the time $\overline{(\cdot)}$ and zonal $[\cdot]$ mean, the total atmospheric methane transport can be decomposed into the transport by the meridional circulation (MMC) and the transport by eddies:

$$[\overline{v}\,\overline{q}] = [\overline{v}][\overline{q}] + [\overline{v'q'}]. \tag{3}$$

Here, v is the meridional velocity, and q is the specific humidity. Eddy terms v' and q' are defined as deviations from the zonal mean and the mean over a time segment of length

1/163 Titan years. The annual mean of the eddy transport is the average of the eddy transports over the time segments. As shown in Fig. S3, the methane transport is dominated by the mean meridional circulation (MMC); eddy transports are much weaker. For Titan's rotation rate, around the solstice, the atmospheric meridional methane transport by MMC reaches deep into the polar region of the summer hemisphere (Fig. S3), and the much weaker eddy transports counteract the transport by the MMC (Fig. S3, left panels). The dominant poleward meridional transport by the MMC and the counteracting eddy transport are also seen in Titan simulation with hemispherically symmetric surface methane reservoirs in the polar regions [*Lora and Mitchell*, 2015]. However, the eddy transports in *Lora and Mitchell* [2015] are mainly confined to the polar regions above the surface methane reservoir and do not change as much with season. This difference in eddy transports may be due to the different spin-up times of the simulations: the simulations in *Lora and Mitchell* [2015] were integrated for 10 Titan years; our simulations are integrated for over 100 Titan years, which we found necessary to obtain a statistically steady state, in which transient eddy transports no longer depend on initial conditions. For Earth's rotation rate, by contrast, atmospheric meridional methane transport by the MMC is largely confined to the equatorial region (Fig. S3, right panels). The much weaker eddy transports are poleward and extend over a broader region.

Text S3: Response of atmospheric meridional methane transport to orbital precession

Following Section 4 in the main text, the response of the atmospheric meridional methane flux to orbital precession $\delta\overline{vq}$ can be decomposed into a dynamic component

$\bar{q}\delta\bar{v}$, a thermodynamic component $\bar{v}\delta\bar{q}$, a quadratic term $\delta\bar{v}\delta\bar{q}$, changes in transient eddy fluxes $\delta\overline{v'q'}$, and the residual (see Equation 2 in the main text). Figure S4 shows how each term in the decomposition of the response of the atmospheric methane flux to orbital precession varies with season.

References

Lora, J. M., and J. L. Mitchell (2015), Titan's asymmetric lake distribution mediated by methane transport due to atmospheric eddies, *Geophys. Res. Lett.*, *42*, 6213–6220.

Neff, J. S., T. A. Ellis, J. Apt, and J. T. Bergstralh (1985), Bolometric albedos of Titan, Uranus, and Neptune, *Icarus*, *62*, 425–432.

Schneider, T., S. D. B. Graves, E. L. Schaller, and M. E. Brown (2012), Polar methane accumulation and rainstorms on Titan from simulations of the methane cycle, *Nature*, *481*, 58–61.

Tomasko, M. G., and P. H. Smith (1982), Photometry and polarimetry of Titan: Pioneer 11 observations and their implications for aerosol properties, *Icarus*, *51*, 65–95.

Tomasko, M. G., B. Bézard, L. Doose, S. Engel, E. Karkoschka, and S. Vinatier (2008), Heat balance in Titan's atmosphere, *Planet. Space. Sci*, *56*, 648–659.

Williams, P. D. (2011), The RAW filter: An improvement to the Robert-Asselin filter in semi-implicit integrations, *Mon. Wea. Rev.*, *139*, 1996–2007.

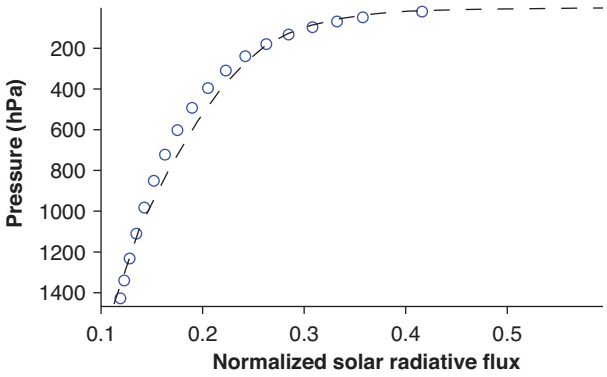

Figure S1. Net solar radiative flux normalized by the incident flux at the top of the atmosphere in the GCM and measured on Titan by the Huygen probe. Dashed line: solar radiative flux inferred from Descent Imager/Spectral Radiometer data obtained by the Huygens probe [*Tomasko et al.*, 2008]. Circles: solar radiative flux at the vertical coordinate levels in the GCM. In the GCM, the normalized solar radiative flux does not depend on latitude or season.

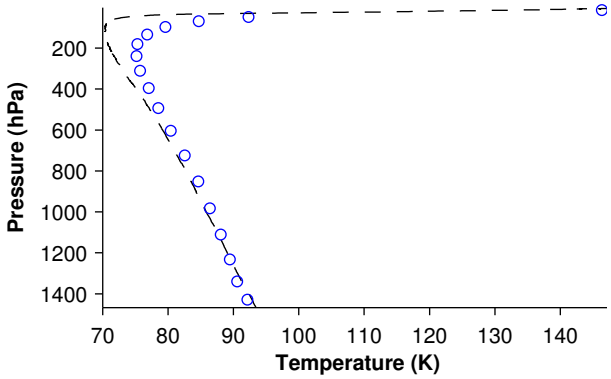

Figure S2. Thermal structure at the Huygens landing site in the GCM and measured on Titan. Dashed line: temperature measured by the Huygen Atmospheric Structure Instrument at 10.2°S on January 14, 2005. Circles: Mean temperature at the corresponding latitude and time at the vertical coordinate levels of the GCM.

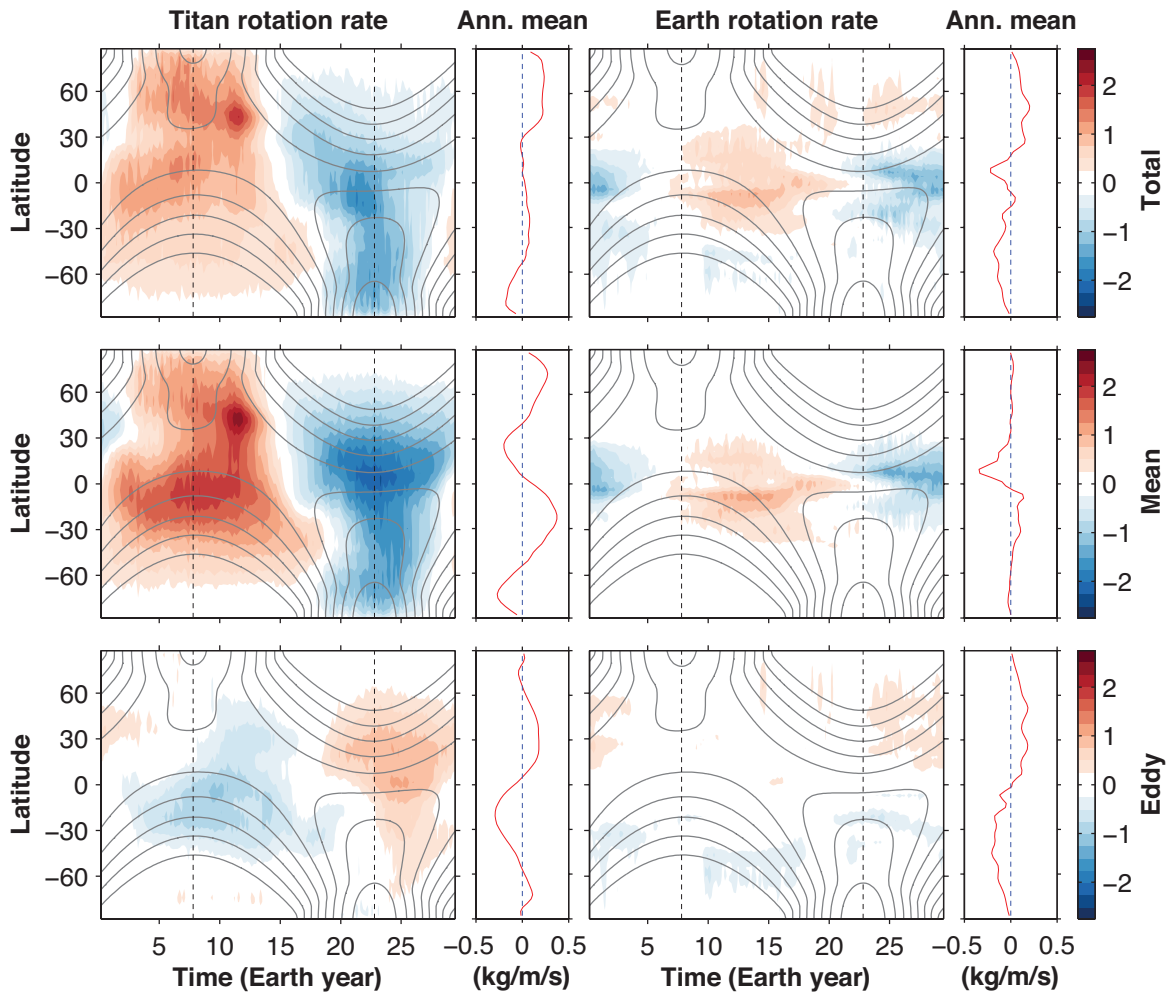

Figure S3. Seasonal evolution of the column integrated atmospheric meridional methane transport. Total atmospheric meridional methane transport $[\overline{vq}]$ (top panels) can be decomposed into the transport by the mean meridional circulation $[\overline{v}][\overline{q}]$ (middle panels) and the eddy transport $[\overline{v'q'}]$ (bottom panels). The grey contours indicate the net solar flux at the surface (contour interval 0.1 W m^{-2}), and the dashed grey lines mark the northern summer solstice (NSS) and the southern summer solstice (SSS). The panels to the right of the contour plots show the annual mean of the quantity in the contour plots (red lines).

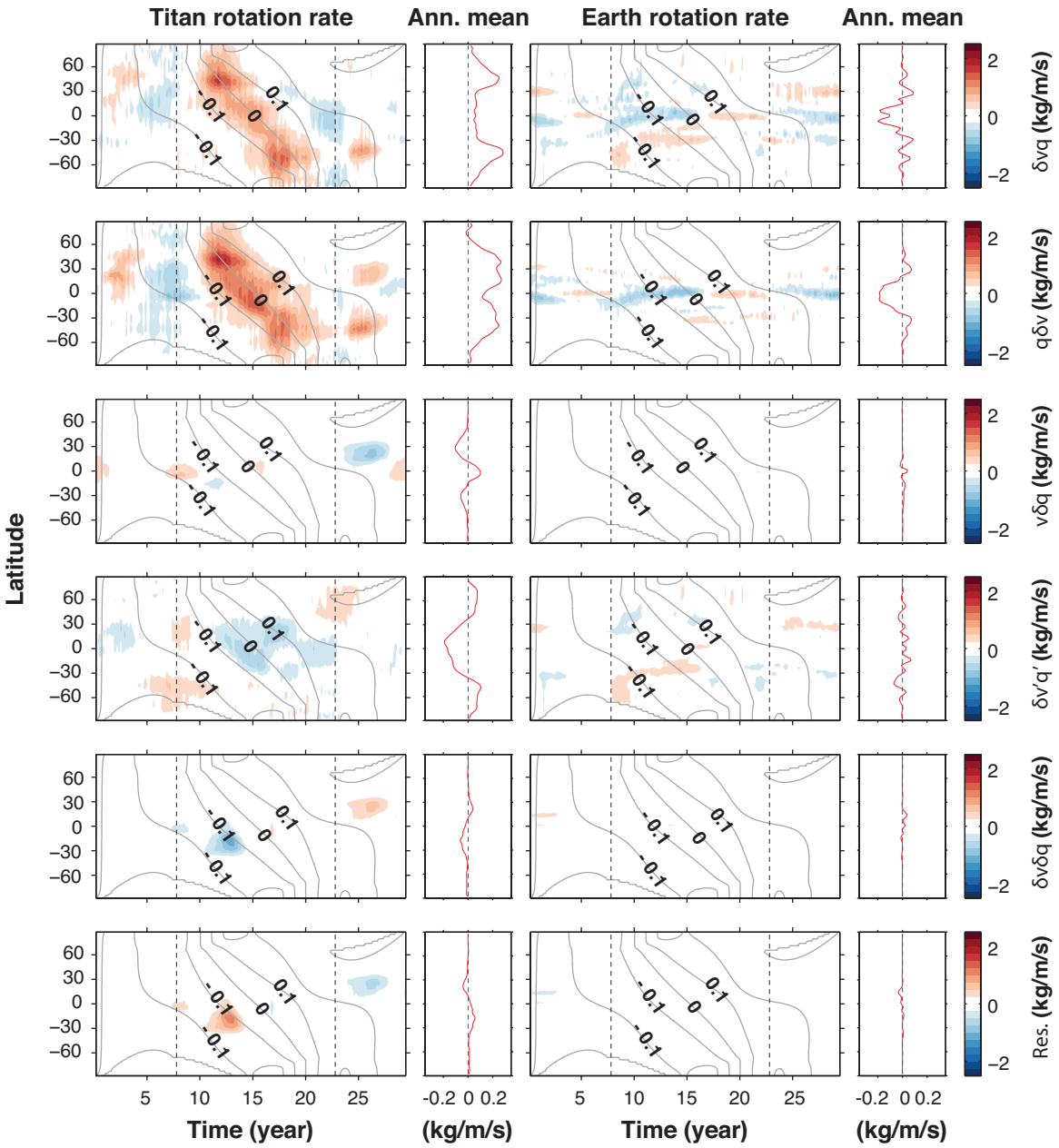

Figure S4. Differences in meridional methane flux (colors) $\delta\overline{v}\overline{q}$ and surface insolation (contours with contour interval 0.1 Wm^{-2}) between the simulations with perihelion in southern summer ($\varpi = 277.7°$) and the simulations with perihelion in the northern summer ($\varpi = 97.7°$). From top to bottom: total difference in meridional methane flux $\delta\overline{v}\overline{q}$; dynamical component $\bar{q}\delta\bar{v}$; thermodynamical component $\bar{v}\delta\bar{q}$; changes in meridional eddy flux $\delta\overline{v'q'}$; quadratic term $\delta\bar{v}\delta\bar{q}$; and residual.